

submitted to ApJ

# Constraints on radiatively inefficient accretion flow models from Eddington ratio distribution of active galactic nuclei

Xinwu Cao

*Shanghai Astronomical Observatory, Chinese Academy of Sciences, 80 Nandan Road,  
Shanghai, 200030, China  
Email: cxw@shao.ac.cn*

and

Ya-Di Xu

*Physics Department, Shanghai Jiaotong University, 1954 Huashan Road, Shanghai,  
200030, China  
Email: ydxu@sjtu.edu.cn*

## ABSTRACT

The radiative efficiencies of accretion flows become significantly lower than that of standard thin disks, if they are accreting at rates lower than a critical accretion rate  $\dot{m}_{\text{crit}}$ . The transition of a standard thin disk to a radiatively inefficient accretion flow (RIAF) is expected to occur, while  $\dot{m} \sim \dot{m}_{\text{crit}}$  ( $\dot{m} = \dot{M}/\dot{M}_{\text{Edd}}$ ). We simulate the distributions of Eddington ratio  $\lambda L_{\lambda}^{\text{B}}/L_{\text{Edd}}$  for active galactic nuclei (AGNs) with such accretion mode transitions in their evolutionary history. It is found that bimodal Eddington ratio distributions appear for most cases. The sources with higher Eddington ratios have standard disks, while the lower component in the Eddington ratio distributions is attributed to the presence of RIAFs in AGNs. Many simulated distributions exhibit a double-peaked feature. The lower peak appears at  $\lambda L_{\lambda}^{\text{B}}/L_{\text{Edd}} \sim 10^{-6} - 10^{-4}$  in the Eddington ratio distributions, only if the RIAFs without winds, or the adiabatic inflow and outflow solution (ADIOS) flows with weak or moderate winds match to standard thin disks at fixed radii larger than one hundred Schwarzschild radii. It is believed that the initial transition radius is small just after the accretion mode transition, and then the transition radius increases with decreasing accretion rate. In such variable transition radius models, a low peak appears in the simulated distributions for almost all cases except the ADIOS flows with strong winds, if

the initial transition radius  $r_{\text{tr},0}$  is greater than ten Schwarzschild radii. For the ADIOS flows with strong winds, the low peak disappears in the Eddington ratio distributions for any cases, though the distributions are still bimodal. Compared with the Eddington ratio distribution for an AGN sample, our simulations can give some constraints on RIAF models.

*Subject headings:* galaxies: active—quasars: general—accretion, accretion disks—black hole physics

## 1. Introduction

Accretion onto massive black holes is believed to power active galactic nuclei (AGNs). The UV/optical continuum emission observed in luminous quasars is attributed to the thermal radiation from the accretion disks surrounding the massive black holes in quasars (e.g., Sun & Malkan, 1989). In recent years, some different approaches are proposed to measure the masses of the central black holes in AGNs (e.g., Peterson 1993; Ferrarese & Merritt 2000; Gebhardt et al. 2000), and the central black hole masses of many AGNs can be measured fairly accurately. It is found that a fraction of luminous AGNs are accreting at extremely high rates. Their bolometric luminosities are around (or even higher than) the Eddington luminosity, for example, the black holes in many narrow-line Seyfert 1 galaxies are believed to be accreting at Eddington (or super-Eddington) rates (e.g., Sulentic et al. 2000; Warner et al. 2004; Bian & Zhao 2004). Besides the luminous AGNs accreting at high Eddington rates ( $\gtrsim 0.01$ ), many nearby low-luminosity AGNs are found to have similar characteristics as those luminous AGNs, but with relatively weaker broad-line emission (Ho et al. 1997). Most of these low-luminosity AGNs are accreting at highly sub-Eddington rates ( $L_{\text{bol}}/L_{\text{Edd}} \ll 0.01$ ). The Eddington ratios of AGNs can spread over more than ten orders of magnitude (from  $\lesssim 10^{-10}$  to more than unity) (e.g., Wu & Cao 2004).

It is believed that standard thin disks (or slim disks) are present in luminous AGNs, while the radiatively inefficient accretion flows (RIAFs) are suggested to be present in those low-luminosity AGNs accreting at relatively low rates. The RIAF models include: advection dominated accretion flow (ADAF), adiabatic inflow-outflow solution (ADIOS), and convection dominated accretion flow (CDAF) models (Narayan & Yi 1994; Blandford & Begelman 1999, 2004; Igumenshchev et al. 2000; Narayan et al. 2000). The densities of the gases in RIAFs are very low, and most gravitational energy released cannot be transferred efficiently to the electrons by Coulomb interactions between ions and electrons in the plasmas. In old version of ADAF models, only Coulomb interactions between ions and electrons is considered, so that most gravitational energy released is carried into the black hole by the accretion flow,

namely, advection dominated. However, this was doubted by Bisnovatyi-Kogan & Lovelace (1997), and they argued that a significant fraction of the viscously dissipated energy (up to  $\delta \sim 1/2$ ) could go into electrons by magnetic reconnection in the presence of magnetic fields in the accretion flow (Bisnovatyi-Kogan & Lovelace 1997, 2000). In this case, the temperatures are still very high, and the accretion flow is subject to outflows, namely, ADIOS model (Blandford & Begelman 1999). In the ADIOS model, a fraction (or even most) of gases in the accretion flow are carried away in the outflows and only a fraction of gases are accreted by the black hole, so the accretion efficiency can still be very low. These RIAF models can successfully explain the observational features of many low-luminosity AGNs (e.g., Narayan et al. 1995; Manmoto et al. 1997; Lasota et al. 1996; Gammie et al. 1999; Yuan et al. 2004). There is a critical accretion rate  $\dot{m}_{\text{crit}}$ , above which the RIAF is suppressed, and a standard thin disk is present. For accretion rates  $\dot{m} > \dot{m}_{\text{crit}}$ , the densities of gases in the flows are so high that the Coulomb interactions can transfer almost all gravitational energy to electrons. The ions and electrons therefore have almost same temperature. The released gravitational energy can be radiated away completely, and the disk is cooled down efficiently. One may expect that an accretion mode transition occurs, while the accretion rate  $\dot{m} \simeq \dot{m}_{\text{crit}}$ . The RIAF may match to a standard thin disk at a certain radius  $R_{\text{tr}}$ . This is required by modelling on a variety of observations on AGNs (e.g., Quataert et al., 1999; Lu & Wang, 2000; Cao, 2003; Kong et al., 2004), and is also predicted by some theoretical model calculations (Abramowicz et al. 1995; Liu et al. 1999; Rozanska & Czerny 2000; Spruit & Deufel 2002). In all these models, the transition radius  $r_{\text{tr}}$  is expected to increase with decreasing accretion rate  $\dot{m}$ .

The evolution of central engines in AGNs is mainly governed by accretion processes. The black hole accretion processes are regulated by the gases supplied near the black hole, i.e., sufficient gases supplied probably lead to a high accretion rate, and vice versa (Springel, Di Matteo, & Hernquist 2005; Di Matteo, Springel, & Hernquist 2005). As the gases being swallowed by the black hole, the accretion rate decreases with time. An AGN will die off, while the gases near the black hole are finally exhausted. It is expected that a standard thin disk is present, if it is accreting at a rate  $\dot{m} > \dot{m}_{\text{crit}}$  (or even a slim disk is expected in the case of  $\dot{m} \gtrsim 0.3$ ) (Abramowicz et al. 1988). The accretion efficiency of a standard thin disk surrounding a non-rotating black hole is around 0.06. As the accretion rate declines with time, the thin disk will transit to a RIAF or a RIAF+standard disk(SD) system, while its accretion rate  $\dot{m}$  approaches the critical value  $\dot{m}_{\text{crit}}$  at a certain time. A luminosity gap measured at a certain wave band is expected, even if the accretion rate declines continuously with time, because the radiative efficiencies of RIAFs are significantly lower than that of standard thin disks and the spectra of RIAFs are significantly different from those of standard thin disks. One may therefore expect a bimodal distribution of Eddington ratio  $\lambda L_{\lambda}/L_{\text{Edd}}$

at a certain waveband for AGNs.

Recently, a bimodal Eddington ratio distribution with double-peaked feature is found by Marchesini et al. (2004) for a sample of radio-loud AGNs, which is suggested to be explained qualitatively by the ADIOS model (Begelman & Celotti 2004). Marchesini et al. (2004) derived the bolometric luminosities for all AGNs from the unresolved optical cores, which may be dominated by the jet emission and some of 3CR FR I galaxies may have obscured bright nuclei (Cao & Rawlings 2004). Although Donato, Sambruna, & Gliozzi (2004) claimed no obscuration in these FRI galaxies from their X-ray observations, most obscured sources discovered by Cao & Rawlings (2004) have not been in their source list or no X-ray core emission detected by *Chandra* or *XMM-Newton* (only 4/13 appears in their list, and two of these four sources have not been detected X-ray compact central cores). The ratios of  $T = L_X/L_{[OIII]}$  for those two sources with detected X-ray compact central cores, 3C346 and 3C348, are 11.2 and 2.7, respectively, which are more close to  $T_{Sy2} = 3.7 \pm 1.1$  for Seyfert 2 galaxies ( $T_{Sy1} = 37.8 \pm 9.6$  for Seyfert 1 galaxies) (Donato, Sambruna, & Gliozzi 2004). This implies that obscuration is important in these two sources. More recently, Jester (2005) pointed that the Eddington ratio distribution derived by Marchesini et al. (2004) may be affected by selection effects. Therefore, it should be cautious on this Eddington ratio distribution derived from a radio-loud AGN sample. In this work, we do not like to be involved in the complexity of how to derive a reliable Eddington ratio distribution from observations. We only intend to investigate the general properties of the Eddington ratio distributions for AGNs by simulations based on different RIAF models, and to explore how the RIAF models can be constrained by a reliable Eddington ratio distribution while available.

## 2. Spectra of radiatively inefficient accretion flows

### 2.1. RIAFs without winds

The transition of an accretion flow from a thin disk to an RIAF occurs, when the accretion rate  $\dot{m}$  decreases to a value below  $\dot{m}_{\text{crit}}$ . The structure of RIAFs is well described by the self-similar solution (Narayan & Yi 1995; Yi 1996). The spectrum of an RIAF,  $L_\lambda(M_{\text{bh}}, \dot{m}, \alpha, \beta)$ , can be calculated based on this self-similar flow structure, if the parameters  $M_{\text{bh}}$ ,  $\dot{m}$ ,  $\alpha$ , and the fraction of the magnetic pressure  $\beta$ , are specified. The parameter  $\beta$ , defined as  $p_m = (1 - \beta)p_{\text{tot}}$ , describes the magnetic field strength of the flow. In this work, we calculate the spectra of RIAFs using the approach proposed by Mahadevan (1997), which is efficient for our numerical simulations and can reproduce the main features of the spectra calculated for the global RIAF structure (Mahadevan 1997). It was pointed out that a

significant fraction of the viscously dissipated energy (up to  $\delta \sim 1/2$ ) could go into electrons by magnetic reconnection, if the magnetic fields in the flow are strong (Bisnovatyi-Kogan & Lovelace 1997, 2000). In most of our calculations, we adopt  $\delta = 1/2$ , while we still present a few simulations by adopting  $\delta = 1/2000$  for comparison.

## 2.2. ADIOS flows

The RIAFs are very hot, and their Bernoulli constants are positive. Therefore, they are supposed to have outflows (Blandford & Begelman 1999; Quataert & Narayan 1999). In this case, the accretion rate  $\dot{m}$  is not constant along radius  $r$  for an ADIOS flow, and it is assumed to be described by

$$\dot{m}(r) = \dot{m}(r_{\text{out}}) \left( \frac{r}{r_{\text{out}}} \right)^{p_w}, \quad (1)$$

where  $\dot{m}(r_{\text{out}})$  is the accretion rate at the outer radius  $r_{\text{out}}$  of the ADIOS flow, and the parameter  $p_w$  describes the wind strength. So, the spectrum of an ADIOS flow can be calculated, while all parameters  $M_{\text{bh}}$ ,  $\dot{m}$ ,  $\alpha$ ,  $\beta$ ,  $r_{\text{out}}$ , and  $p_w$ , are specified (Chang et al. 2002; Wu & Cao 2005).

## 3. Spectra of standard disks

For a standard thin disk, the flux due to viscous dissipation in unit surface area is

$$F_{\text{vis}}(R) \simeq \frac{3GM_{\text{bh}}\dot{M}}{8\pi R^3} \left[ 1 - \left( \frac{3R_{\text{G}}}{R} \right)^{1/2} \right], \quad (2)$$

where  $R_{\text{G}} = 2GM_{\text{bh}}/c^2$ . The local disk temperature of the thin cold disk is

$$T_{\text{disk}}(R) = \frac{F_{\text{vis}}^{1/4}(R)}{\sigma_{\text{B}}^{1/4}}, \quad (3)$$

by assuming local blackbody emission. In order to calculate the disk spectrum, we include an empirical color correction for the disk thermal emission as a function of radius. The correction has the form (Chiang 2002)

$$f_{\text{col}}(T_{\text{disk}}) = f_{\infty} - \frac{(f_{\infty} - 1)[1 + \exp(-\nu_{\text{b}}/\Delta\nu)]}{1 + \exp[(\nu_{\text{p}} - \nu_{\text{b}})/\Delta\nu]}, \quad (4)$$

where  $\nu_p \equiv 2.82k_B T_{\text{disk}}/h$  is the peak frequency of blackbody emission with temperature  $T_{\text{disk}}$ . This expression for  $f_{\text{col}}$  goes from unity at low temperatures to  $f_{\infty}$  at high temperatures with

a transition at  $\nu_b \approx \nu_p$ . Chiang (2002) found that  $f_\infty = 2.3$  and  $\nu_b = \Delta\nu = 5 \times 10^{15}$  Hz can well reproduce the model disk spectra of Hubeny et al. (2001). The disk spectra can therefore be calculated by

$$L_\nu = 32\pi^2 \left( \frac{GM_{\text{bh}}}{c^2} \right)^2 \frac{h\nu^3}{c^2} \int_{r_{\text{in}}}^{\infty} \frac{rdr}{f_{\text{col}}^4 [\exp(h\nu/f_{\text{col}}k_B T_{\text{disk}}) - 1]}, \quad (5)$$

where  $r_{\text{in}} = R_{\text{in}}/R_G$  is the inner radius of the standard disk. At a high accretion rate,  $\dot{m} > \dot{m}_{\text{crit}}$ , the standard thin disk extends to the minimum stable orbit of the black hole,  $r_{\text{in}} = 3$ , for a non-rotating hole. For a RIAF+SD system, the spectrum emitted from the standard disk region can be calculated by using the transition radius  $r_{\text{tr}}$  ( $r_{\text{tr}} = R_{\text{tr}}/R_G$ ) instead of  $r_{\text{in}}$  as the lower integral limit in Eq. (5).

#### 4. Transition radius $R_{\text{tr}}$ between RIAF and standard thin disk

In this work, we assume the transition from a standard thin disk to a RIAF to occur whenever  $\dot{m} \lesssim \dot{m}_{\text{crit}}$ , i.e., so-called "strong principle". The RIAF is naturally expected to match a standard thin disk at a large radius  $r_{\text{tr}}$ . The detailed physics, causing such a transition of a standard thin disk to a RIAF, is still unclear. It is suggested that the standard thin disk transits to a RIAF truncated at an initial transition radius  $r_{\text{tr},0}$ , while  $\dot{m} = \dot{m}_{\text{crit}}$ , and the transition radius  $r_{\text{tr}}$  varies with the dimensionless accretion rate  $\dot{m}$  as

$$r_{\text{tr}} \propto \dot{m}^{-p}, \quad (6)$$

where  $p = 2$  is predicted, based on the scenario of transition triggered by the thermal instability, by Abramowicz et al. (1995); and  $p \simeq 0.8 - 1.3$  is expected by the disk evaporation induced transition scenarios (Liu et al. 1999; Rozanska & Czerny 2000; Spruit & Deufel 2002). In either one of these transition scenarios, the transition radius  $r_{\text{tr}}$  always increases with decreasing accretion rate  $\dot{m}$ . However, the initial transition radius  $r_{\text{tr},0}$ , while  $\dot{m} \sim \dot{m}_{\text{crit}}$ , is still unknown. We adopt  $r_{\text{tr},0}$  as a parameter in our simulations, and try to constrain it from the comparisons of the simulated Eddington ratio distributions with the observed distribution.

#### 5. Numerical simulations of Eddington ratio distribution

In order to simulate the distributions of Eddington ratio  $\lambda L_\lambda / L_{\text{Edd}}$  for AGNs, we need to know how the accretion rate  $\dot{m}$  evolves with time. Unfortunately, this remains to be an

unsolved issue. though the exponentially time-dependent accretion rate  $\dot{m}(t)$  was widely employed in many previous works (e.g., Park & Vishniac, 1990; Haiman & Loeb, 1998; Kauffmann & Haehnelt, 2000). McMillan, Lightman, & Cohn (1981) found accretion rate  $\dot{m}(t) \propto t^{-2}$ , if the gases accreted by the black hole are assumed to be supplied by stellar collisions or tidal disruptions in a dense star system surrounding the black hole. Compared with exponentially time-dependent accretion rate, this form of accretion rate changes very slowly with time. Many quasar evolution model calculations showed that the exponentially time-dependent quasar light curve (or simply a step function quasar light curve) can well reproduce the observed quasar luminosity functions (Haiman & Loeb, 1998; Wyithe & Loeb, 2002). Recently, the numerical simulations on the quasar activity triggered by the galaxy merger showed that the quasar accretion rate curve is very complicated (Springel, Di Matteo, & Hernquist 2005; Di Matteo, Springel, & Hernquist 2005). In their model, the gases near the black hole are blown away by the bright quasar radiation, and then accretion rate declines rapidly to switch off the quasar activity. The simple exponentially time-dependent accretion rate is unable to describe the whole accretion rate curve suggested by their simulations. One important feature of their simulated quasar accretion rate curve is a rapid drop from near Eddington rate to substantially low rate within a short timescale. At least, an exponentially time-dependent form of accretion rate can describe this sharply drop of accretion rate fairly well, if a suitable value of  $t_Q$  is tuned. So, in order to describe the whole light curve, one has to employ another form of time-dependent accretion rate to describe the bright phase of quasar accretion rate curve. However, in most of our simulations, we assume the dimensionless accretion rate  $\dot{m}$  to decline exponentially with time:

$$\dot{m} = \dot{m}(t = 0)e^{-t/t_Q}, \quad (7)$$

for the whole quasar accretion rate curve, where  $t_Q$  is the  $e$ -fold accretion time scale. The resulted distribution is only dependent of the form of accretion rate, while it does not depend on the values of  $t_Q$  for individual sources, i.e., the resulted distribution is not affected, even if every sources have different values of  $t_Q$ , but obey the same time-dependent form of accretion rate. So, this simple exponentially time-dependent accretion rate may not well describe the sources accreting at higher rates, and may affect the higher ratio parts in the distribution, while the profile of the Eddington ratio distribution at lower ratios, corresponding to the sources at the stage of accretion rate declining rapidly from near Eddington rate to substantially low rate, will not be affected. In this work, we are mainly interested in the Eddington distribution at low ratios corresponding to RIAFs, so that our main conclusions will not be altered by this simple exponential accretion rate curve for the whole quasar life. In our calculations, we assume  $\dot{m}(t = 0) = 1$ . Strictly speaking, the accretion rate  $\dot{m}$  could be higher than unity. However, in this work, we are focusing on the accretion mode transition from a standard thin disk to a RIAF, so the assumption of  $\dot{m}(t = 0) = 1$  will not affect our main

conclusions. We also simulate the Eddington ratio distribution for the case of  $\dot{m}(t) \propto t^{-2}$ , to explore how the resulted Eddington ratio distribution is altered by this slowly evolving accretion rate.

There is a critical accretion rate  $\dot{m}_{\text{crit}}$ , above which the standard thin disk extends to the minimum stable orbit of the black hole. The critical accretion rate  $\dot{m}_{\text{crit}}$  depends sensitively on the viscosity parameter  $\alpha$ . A rough estimate gives an analytic relation between  $\alpha$  and  $\dot{m}_{\text{crit}}$ :  $\dot{m}_{\text{crit}} \simeq 0.28\alpha^2$  (Mahadevan 1997). In this work, the critical accretion rate  $\dot{m}_{\text{crit}}$  is derived from the numerical calculations of the RIAF structure, for given parameters  $\alpha$  and  $\beta$ . We change the values of  $\dot{m}$  to find a maximal value:  $\dot{m}_{\text{crit}}$  for the presence of two-temperature accretion flow structure. In most our simulations, we adopt  $\beta = 0.5$ , i.e., equipartition between the gas and magnetic pressure, and we also explore the situation for which the value of  $\beta$  being randomly distributed in the range of  $0.5 - 1$ . While the accretion rate  $\dot{m}$  becomes lower than the critical rate  $\dot{m}_{\text{crit}}$ , a RIAF may be present in the inner region of the disk, and a RIAF+SD system is formed in the AGN. The spectrum of this RIAF+SD system consists of the emission from the inner RIAF and the outer standard thin disk region. The spectrum emitted from the inner RIAF can be calculated, as described in Sects. 2.1 and 2.2, for RIAFs with or without winds, respectively. The spectrum emitted from the standard thin disk or the outer standard thin disk region in the RIAF+SD system can be calculated as described in Sect. 3. We can therefore calculate the spectral evolution of the accretion flow in an AGN. The distributions of Eddington ratio can be simulated, by calculating of spectral evolution for a large number of AGNs, for different values (distributions) of transition radius  $r_{\text{tr}}$ ,  $\beta$ , or/and viscosity parameter  $\alpha$ , for RIAFs either with winds or without winds, respectively.

## 6. Numerical results

### 6.1. Spectral evolution of RIAF+SD systems

The spectrum of a standard disk is mainly determined by its temperature, which depends weakly on the black hole mass as  $\propto M_{\text{bh}}^{1/4}$ . The gases in RIAFs are nearly virialized, and their structure is almost independent of the black hole mass. So, the ratio  $\lambda L_{\lambda}^{\text{B}}/L_{\text{Edd}}$  of the RIAF+SD system is insensitive to black hole mass  $M_{\text{bh}}$ . We calculate the ratio of  $B$ -band luminosity to Eddington luminosity  $\lambda L_{\lambda}^{\text{B}}/L_{\text{Edd}}$  adopting  $M_{\text{bh}} = 5 \times 10^8 M_{\odot}$ , because most AGNs have black hole masses in the range of  $10^8 - 10^9 M_{\odot}$  (e.g., McLure, & Jarvis, 2004). In Fig. 1, the spectral evolution of RIAF+SD systems is plotted for different viscosity parameters  $\alpha$ , and transition radii  $r_{\text{tr}}$ . The luminosity drops sharply, while  $\dot{m} \leq \dot{m}_{\text{crit}}$ , if a pure RIAF (without an outer standard thin disk region) is present after the accretion

mode transition, or the RIAF is truncated at a large radius  $r_{\text{tr}}$  ( $\gtrsim$  several hundred) for the RIAF+SD system.

The standard disk may not be truncated to an RIAF at a fixed radius. The transition radius  $r_{\text{tr}}$  may vary with accretion rate  $\dot{m}$ . Some theoretical investigations suggest  $r_{\text{tr}} \propto \dot{m}^{-p}$  (Abramowicz et al. 1995; Liu et al. 1999; Rozanska & Czerny 2000; Spruit & Deufel 2002). We plot the spectral evolution of RIAF+SD systems with variable transition radii  $r_{\text{tr}}$  in Fig. 2. It is found that the spectral evolution of RIAF+SD systems is similar to pure-RIAF cases, except within a period of time  $\sim 1 - 2t_{\text{Q}}$  soon after the accretion mode transition. This is caused by the fact that the transition radius  $r_{\text{tr}}$  increasing rapidly with decreasing accretion rate  $\dot{m}$  just after the accretion mode transition.

In Fig. 3, we present the light curves for ADIOS flows with different parameters. The results for ADIOS flows are qualitatively similar to the RIAFs without winds. If the winds are stronger, i.e., larger  $p_{\text{w}}$ , the emission from the ADIOS flow declines more rapidly with time.

## 6.2. Distributions of Eddington ratio $\lambda L_{\lambda}^{\text{B}}/L_{\text{Edd}}$

We simulate the distributions of Eddington ratio  $\lambda L_{\lambda}^{\text{B}}/L_{\text{Edd}}$  for different transition radii  $r_{\text{tr}}$  and different viscosity parameters  $\alpha$  in Fig. 4. The bimodal distributions are present for most cases. The sources in the component with higher Eddington ratios have standard disks. In the case of a standard thin disk transiting to a pure-RIAF or to a RIAF truncated to a standard thin disk at a large radius ( $r_{\text{tr}} \gtrsim 100$ ), a peak appears at a low Eddington ratio:  $\lambda L_{\lambda}^{\text{B}}/L_{\text{Edd}} \sim 10^{-5.5} - 10^{-4.5}$ , in the simulated distributions for  $\alpha = 0.1$  or 1 (see Fig. 4). In the case of  $\alpha = 0.01$ , only a small hump appears for any transition radius adopted (see the lower panel of Fig. 4).

The exact values of viscosity parameters  $\alpha$  of the accretion flows in AGNs are still unknown. The viscosity in accretion flows is supposed to be attributed to turbulence, so the viscosity parameter  $\alpha$  is required to be less than unity (Shakura & Sunyaev 1973). We simulate the Eddington ratio distributions in the upper panel of Fig. 5, assuming  $\alpha$  to be randomly distributed in the range of 0 – 1 for all AGNs. It is found that the distributions have similar features as those for  $\alpha = 0.1$  or 1, i.e., a peak at the low Eddington ratio  $\lambda L_{\lambda}^{\text{B}}/L_{\text{Edd}} \sim 10^{-5.5} - 10^{-4.5}$  appears for pure-RIAFs or the RIAFs truncated at a large radius  $r_{\text{tr}} \gtrsim 200$ . The three-dimensional MHD simulations suggest the viscosity parameter  $\alpha$  in the accretion flows to be  $\sim 0.1$  (Armitage 1998), or  $\sim 0.05 - 0.2$  (Hawley & Balbus 2002). If this is the case, the viscosity parameter is expected to be in a narrower range than 0 – 1.

So, we perform similar simulations for the viscosity parameter  $\alpha$  in the range of 0.1 – 0.3. The distributions are similar to those for  $\alpha$  in the range of 0 – 1 (see the lower panel of Fig. 5).

As discussed in Sect. 4, the transition radius  $r_{\text{tr}}$  may vary with accretion rate  $\dot{m}$  as  $r_{\text{tr}} \propto \dot{m}^{-p}$ . We simulate the Eddington ratio distributions for this variable transition radius model in Fig. 6. We find that an obvious peak appears at  $\lambda L_{\lambda}^{\text{B}}/L_{\text{Edd}} \sim 10^{-5} - 10^{-4.5}$  for either  $p = 1$  or 2, even if a small initial transition radius  $r_{\text{tr},0} = 10$  is adopted.

The simulations of Eddington ratio distribution are carried out for ADIOS cases in Figs. 7–9. In Fig. 7, we find no obvious low peak appears for strong wind cases ( $p_{\text{w}} = 0.9$ ) adopting a fixed transition radius  $r_{\text{tr}} = 100$  or 200, either for  $\alpha$  in the range of 0 – 1 or 0.1 – 0.3. For weak ( $p_{\text{w}} = 0.1$ ) or moderate winds ( $p_{\text{w}} = 0.4$ ), a low peak appears in the simulated Eddington ratio distributions for a fixed transition radius  $r_{\text{tr}} = 200$ . In the case of  $r_{\text{tr}} = 100$ , a low peak appears only for the flows with weak winds ( $p_{\text{w}} = 0.1$ ).

The results for the accretion flows with variable transition radii are plotted in Figs. 8 and 9, for  $r_{\text{tr},0} = 10$  and 50, respectively. In both of these two cases, we have not found an obvious lower peak in the distributions for strong wind cases ( $p_{\text{w}} = 0.9$ ).

In all the previous simulations, equipartition between the magnetic and gas pressure is assumed, i.e.,  $\beta = 0.5$  is adopted in the calculations. In Figs. 10 and 11, we simulate the Eddington ration distribution for the case with  $\beta$  being randomly distributed in the range of 0.5 – 1. The results are quite similar to those for the fixed value of  $\beta = 0.5$ .

We also perform simulations for the cases of  $\delta = 1/2000$  in Fig. 12, which corresponds to the old version of ADAF models, and it is found that a low peak appears only for the cases of  $p = 2$  at  $\sim 10^{-6}$ .

It is still unclear how the accretion rate  $\dot{m}$  evolves with time. We also simulate the Eddington ration distributions with an power-law time-dependent accretion rate  $\dot{m}(t) = \dot{m}_{\text{crit}}(t=0)(1+t/t_{\text{Q}})^{-\xi}$ , where  $\xi = 2$  is adopted. This power-law time-dependent accretion rate evolves much slowly with time compared with the exponential one. As the accretion rate varies with time slowly, so many sources with low Eddington ratios are expected in the simulated Eddington ratio distributions (see Fig. 13).

## 7. Discussion

The ADIOS flow is usually fainter than the RIAF without winds, if both of them have the same accretion rate at their outer radius (see Fig. 3), because less gases are accreted and

a fraction of gravitational energy released in the ADIOS flow is carried away by the outflow. For an RIAF+SD system, its optical emission is mostly from the outer standard accretion thin disk region, if its accretion rate  $\dot{m}$  is close to the critical one  $\dot{m}_{\text{crit}}$  and the transition radius is not very large. For large transition radius, the temperature of the standard thin disk region is very low, and the optical emission is dominantly from the inner RIAF (see Figs. 1-3). A luminosity gap is found at  $\dot{m} \sim \dot{m}_{\text{crit}}$ , which is obvious, if the transition radii  $r_{\text{tr}}$  is large.

Most simulations of Eddington ratio distribution based on the RIAF+SD scenario show a bimodal feature, whereas only a fraction of them have peaked structure at low Eddington ratios ( $\sim 10^{-6} - 10^{-4}$ ). For fixed transition radius model, we find bimodal distributions (a hump or peaked structure) for almost all cases without winds (either small or large transition radii), while peaked structure appears in the distributions only for those simulations with relatively large transition radii, i.e.,  $r_{\text{tr}} \gtrsim 100$  (see Figs. 4 and 5). This can be naturally understood, as the luminosity gap increases with transition radius  $r_{\text{tr}}$ . Unlike the fixed transition radius model, for the variable transition radius model, the peaked structure always appears even if the initial transition radius  $r_{\text{tr},0}$  is as small as ten (see Fig. 6), either for  $p = 1$  or  $2$ . This is because the transition radius increases with decreasing accretion rate very rapidly in the transition radius model, so a luminosity gap appears, though not sharp, even for a small initial transition radius  $r_{\text{tr},0}$  (see Fig. 2).

For ADIOS flows, no peaked structure (only a hump) appears in the simulated distributions, if the winds are strong ( $p_w = 0.9$ ). The peaked structures are found in the simulated distributions for weak or moderate wind cases, while  $r_{\text{tr}} \gtrsim 200$ . For a smaller transition radius  $r_{\text{tr}} = 100$ , the peaked structure is found only for weak wind cases ( $p_w = 0.1$ ). Unlike the RIAFs without winds, no peaked structures appear in the simulated distributions for strong wind cases ( $p_w = 0.9$ , even if  $r_{\text{tr},0} = 50$ ) is adopted. This can be understood, because no peaked structure is present for strong wind cases, even if the fixed  $r_{\text{tr}}$  is as large as several hundred. For weak or moderate wind cases, peaked structures are always present even for  $r_{\text{tr},0} = 10$ . In Figs. 10 and 11, we present the simulations for  $\beta$  being randomly distributed in the range of  $0.5 - 1$ , and find that peaked structure is present only for weak wind cases.

A large transition radius makes a luminosity gap during the spectral evolution of AGNs, so the peaked structure is always easily present for large transition radii. However, this alone is not sufficient to reproduce peaked Eddington ratio distribution. The number counts in unit logarithm of Eddington ratio are proportional to  $(d \log l/dt)^{-1}$ , where  $l = \lambda L_{\lambda}^{\text{B}}/L_{\text{Edd}}$ . For ADIOS flows with strong winds, their emission is faint and decreases rapidly with time, so no peaked structure appears for strong wind cases. For the RIAFs without winds or with moderate winds ( $p_w \lesssim 0.4$ ), the light curves are rather flat after the accretion mode transition

(see Fig. 3). The AGNs evolve slowly at the time shortly after the accretion mode transition, which increases the number counts of AGNs at the Eddington ratio of  $\sim 10^{-6} - 10^{-4}$ , as the number counts are proportional to  $(d \log l/dt)^{-1}$ . So, this peak in the Eddington ratio distributions is indeed caused by this spectral characteristics of RIAFs without winds or with moderate winds. It means that any peaked structure at low ratios in the distributions should be attributed to the characteristics of RIAFs without winds or with only moderate winds, while only a hump appears if the RIAFs in AGNs have strong winds.

We also simulate the distributions for old ADAF models by setting  $\delta = 1/2000$ , and find peaked structure only for the flow without winds or with very weak winds in some cases. This is caused by the fact that the old-version ADAFs are fainter than those RIAFs with a large  $\delta$ . Finally, we simulate the cases with a power-law time-dependent accretion rate, and find many sources with very low Eddington ratios in the simulated distributions. This seems to be inconsistent with the observations of any AGN sample, and this slowly evolving accretion rate also disagrees with the numerical simulations on AGN activity (Springel, Di Matteo, & Hernquist 2005).

In summary, our simulations show that no peak structure appears at low Eddington ratio for the RIAFs with strong winds, while a peak at the low ratio around  $10^{-5.5} - 10^{-4.5}$  appears in the Eddington ratio distributions, only if one of the following conditions, for the accretion flows after the accretion mode transition, is satisfied:

1. pure-RIAFs without winds;
2. the RIAFs without winds, or ADIOS flows with weak or moderate winds truncated at large radii (more than one hundred Schwarzschild radii);
3. the RIAFs without winds, or ADIOS flows with weak or moderate winds, and the initial transition radii are around (or larger than) ten Schwarzschild radii, for variable transition radius models.

The distribution of  $L_{\text{bol}}/L_{\text{Edd}}$  for a radio-loud AGN sample exhibits a bimodal feature with a lower peak at  $\sim 10^{-4}$  (Marchesini et al. 2004). As discussed in Sect. 1, it should be cautious on this distribution. However, we can now tentatively compare their results with our simulations, before a more reliable Eddington ratio distribution is available from observations. In their work, they adopted a conversion factor of 10 to convert the observed core optical luminosities at  $B$ -band to bolometric luminosities for all AGNs in their sample (Elvis 2002). The Eddington ratio distribution of this radio-loud AGN sample is in general consistent with our simulations, if any one of the conditions listed above is satisfied. This implies that most (if not all) RIAFs in AGNs should not have strong winds. Whether there is a peak appears at low Eddington ratio, or/and the location of such a peak if it does, in the

observed Eddington ratio distribution for AGNs, can be used to constrain some important parameters of different RIAF models and even the accretion history of RIAFs in AGNs.

In all our present calculations, we implicitly assume the accretion mode transition to be short compared with the quasars' life timescale. The timescale of the transition from the standard thin disk to an RIAF is roughly comparable with the viscous timescale of the disk. The viscous timescale is given by

$$t_{\text{vis}} \sim \frac{R^2}{\nu} = \frac{R^2}{\alpha c_s H}, \quad (8)$$

where  $\alpha$ -viscosity is adopted,  $c_s$  is the sound speed, and  $H$  is the scale-height of the disk. Substituting  $c_s = H\Omega_K$  into Eq. (8), we obtain

$$t_{\text{vis}} \sim 4.41 \times 10^{-5} \alpha^{-1} m_8 r^{3/2} \left( \frac{H}{R} \right)^{-2} \text{yr}, \quad (9)$$

where  $m_8 = M_{\text{bh}}/10^8 M_{\odot}$ . Adopting a typical value of viscosity:  $\alpha = 0.1$ , we have  $\dot{m}_{\text{crit}} \sim 0.005$ . For a standard thin disk,  $H/R \sim \dot{m}$ , so we get  $t_{\text{vis}} \sim 5.6 \times 10^4$  years, for  $r_{\text{tr}} = 100$ . In the variable transition radius model, the RIAF transited from a standard thin accretion disk has an initial transition radius  $r_{\text{tr},0}$ , which could be very small. For  $r_{\text{tr},0} = 10$ , the viscous timescale  $t_{\text{vis}} \sim 1.8 \times 10^3$  years. Compared with the typical quasar life timescale of  $\sim 10^8$  years (e.g., Yu & Tremaine 2002), the timescale of the accretion mode transition is always short, which has not been affected our present results.

The standard thin disk model is valid, only for accretion rates  $\dot{m} \lesssim 0.3$  (Laor & Netzer 1989). In this work, we calculate the spectral evolution of accretion disks using standard thin disk models, while the black holes are accreting at relatively high rates ( $\dot{m} \sim 1$ ). The slim disks are probably present in those AGNs accreting at such high rates (e.g., Wang et al. 1999). In this work, we are focusing the low peaks in the Eddington ratio distributions, which are closely related with the properties of RIAFs accreting at low rates. So, our calculations, based on standard thin disk models even for  $\dot{m} \gtrsim 0.3$ , will not affect any conclusions on the Eddington ratio distributions at low ratios discussed in this work.

We thank M.C. Begelman for his helpful comments and suggestions on the original manuscript, A. Loeb for the explanation on their quasar evolution models, and R. Narayan for helpful conversation. This work is supported by the National Science Fund for Distinguished Young Scholars (grant 10325314), NSFC (grants 10173016; 10333020), and the NKBRSPF (grant G1999075403).

## REFERENCES

Abramowicz, M. A., Chen, X., Kato, S., Lasota, J. -P., & Regev, O. 1995, ApJ, 438, L37

Abramowicz, M. A., Czerny, B., Lasota, J. P., & Szuszkiewicz, E. 1988, ApJ, 332, 646

Armitage P.J. 1998, ApJ, 501, L189

Begelman, M. C., & Celotti, A. 2004, MNRAS, 352, L45

Bian, W., & Zhao, Y. 2004, MNRAS, 352, 823

Bisnovatyi-Kogan, G. S., & Lovelace, R. V. E., 1997, ApJ, 486, L43

Bisnovatyi-Kogan, G. S., & Lovelace, R. V. E., 2000, ApJ, 529, 978

Blandford, R. D., & Begelman, M. C. 1999, MNRAS, 303, L1

Blandford, R. D., & Begelman, M. C. 2004, MNRAS, 349, 68

Cao, X., 2003, ApJ, 599, 147

Cao, X., & Rawlings, S., 2004, MNRAS, 349, 1419

Chang H.Y., Choi C.S., & Yi I. 2002, AJ, 124, 1948

Chiang, J. 2002, ApJ, 572, 79

Di Matteo, T., Springel, V., & Hernquist, L., 2005, Nature, 433, 604

Donato, D., Sambruna, R. M., & Gliozzi, M., 2004, ApJ, 617, 915

Elvis, M. 1994, ApJS, 95, 1

Ferrarese, L., & Merritt, D. 2000, ApJ, 539, L9

Gammie, C. F., Narayan, R., & Blandford, R. 1999, ApJ, 516, 177

Gebhardt, K. et al. 2000, ApJ, 539, L13

Haiman, Z., & Loeb, A., 1998, ApJ, 503, 505

Hawley, J.F., & Balbus, S.A. 2002, ApJ, 573, 738

Ho, L. C., Filippenko, A. V., Sargent, W. L. W., Peng, C. Y. 1997, ApJS, 112, 391

Hubeny, I., Blaes, O., Krolik, J. H., & Agol, E. ApJ, 559, 680

Igumenshchev, I. V., Abramowicz, M. A., & Narayan, R. 2000, *ApJ*, 537, L27

Jester, S., 2005, *ApJ*, in press, astro-ph/0502394

Kauffmann, G., & Haehnelt, M., 2000, *MNRAS*, 311, 576

Kong, M.Z., Wu, X. -B., Han, J. L., & Mao, Y. F. 2004, *ChJAA*, 4, 518

Laor, A., & Netzer, H. 1989, *MNRAS*, 238, 897

Lasota, J.-P., Abramowicz, M. A., Chen, X., Krolik, J., Narayan, R., & Yi, I. 1996, *ApJ*, 462, 142

Liu, B. F., Yuan, W., Meyer, F., Meyer-Hofmeister, E., & Xie, G. Z. 1999, *ApJ*, 527, L17

Lu, Y., & Wang, T. 2000, *ApJ*, 537, L103

Mahadevan, R. 1997, *ApJ*, 477, 585

Manmoto, T., Mineshige, S., & Kusunose, M. 1997, *ApJ*, 489, 791

Marchesini, D., Celotti, A., & Ferrarese, L. 2004, *MNRAS*, 351, 733

McLure, R. J., & Jarvis, M. J. 2004, *MNRAS*, 353, L45

McMillan, S.L.W., Lightman, A.P., & Cohn, H., 1981, *ApJ*, 251, 436

Narayan, R., Igumenshchev, I. V., & Abramowicz, M. A. 2000, *ApJ*, 539, 798

Narayan, R., & Yi, I. 1994, *ApJ*, 428, L13

Narayan, R., & Yi, I. 1995, *ApJ*, 452, 710

Narayan, R., Yi, I., & Mahadevan, R. 1995, *Nature*, 374, 623

Park, S.J., & Vishniac, E.T., 1990, *ApJ*, 353, 103

Peterson, B. M. 1993, *PASP*, 105, 247

Quataert, E., di Matteo, T., Narayan, R., & Ho, L. C. 1999, *ApJ*, 525, L89

Quataert, E., & Narayan, R. 1999, *ApJ*, 520, 298

Rozanska, A., & Czerny, B. 2000, *A&A*, 360, 1170

Shakura, N. I., & Sunyaev, R. A. 1973, *A&A*, 24, 337

Springel, V., Di Matteo, T., & Hernquist, L., 2005, MNRAS, in press (astro-ph/0411108)

Spruit, H. C., & Deufel, B. 2002, A&A, 387, 918

Sulentic, J. W., Zwitter, T., Marziani, P., & Dultzin-Hacyan, D. 2000, ApJ, 536, L5

Sun, W. -H., & Malkan, M. A. 1989, ApJ, 346, 68

Wang, J.-M., Szuszkiewicz, E., Lu, F.-J., & Zhou, Y.-Y., 1999, ApJ, 522, 839

Warner, C., Hamann, F., & Dietrich, M. 2004, ApJ, 608, 136

Wu, Q., & Cao, X. 2005, ApJ, 621, 130

Wyithe, J.S.B., & Loeb, A., 2002, ApJ, 581, 886

Yi, I. 1996, ApJ, 473, 645

Yu, Q., & Tremaine, S., 2002, MNRAS, 335, 965

Yuan, F., Quataert, E., & Narayan, R., 2004, ApJ, 606, 894

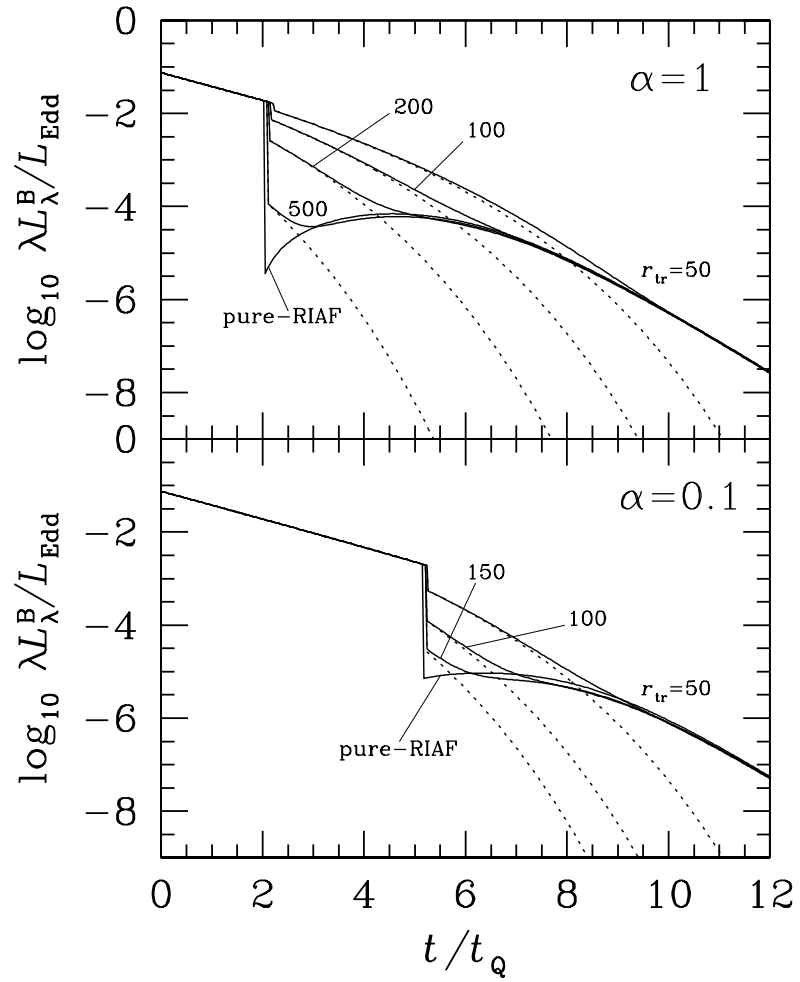


Fig. 1.— Spectral evolution of RIAF+SD systems with different transition radii  $r_{\text{tr}}$ . The dotted lines represent the emission from the outer standard thin disk regions. The upper panel is for  $\alpha = 1$ , while the lower panel is for  $\alpha = 0.1$ .

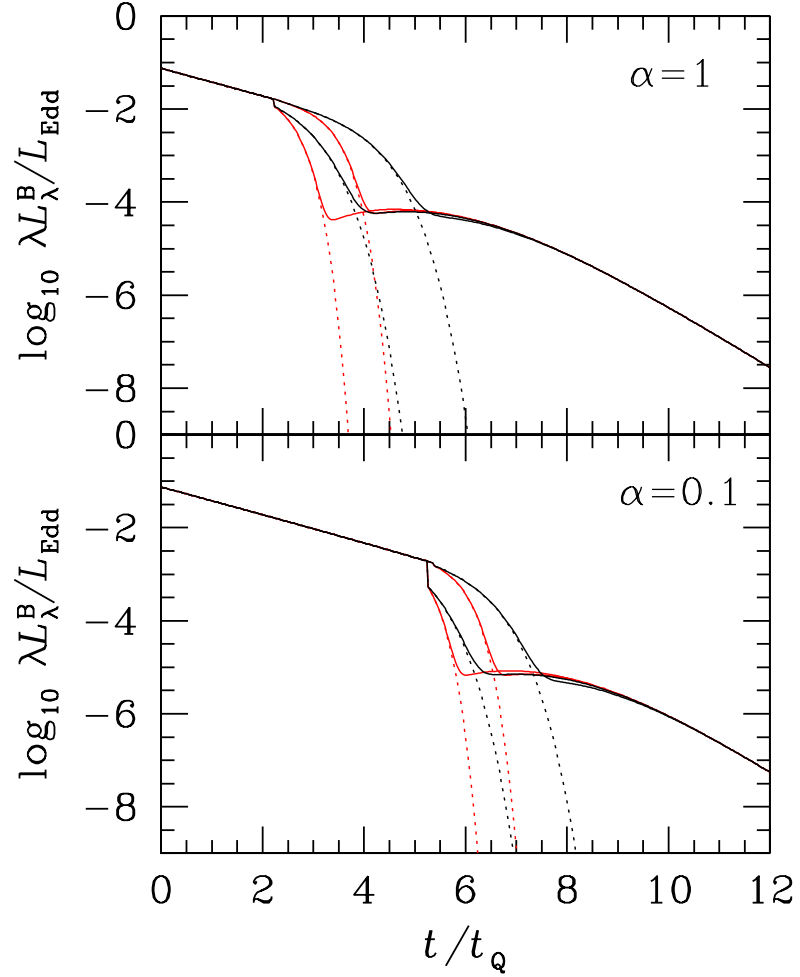


Fig. 2.— Spectral evolution of RIAF+SD systems with different initial transition radii  $r_{\text{tr},0}$ . The transition radius  $r_{\text{tr}}$  is assumed to vary with accretion rate:  $r_{\text{tr}} = r_{\text{tr},0}(\dot{m}/\dot{m}_{\text{crit}})^{-p}$ . The black lines correspond to  $p = 2$ , while the red lines correspond to  $p = 1$ . The upper line is for  $r_{\text{tr},0} = 10$ , and the lower one is for  $r_{\text{tr},0} = 50$ . The dotted lines represent the emission from the outer standard thin disk regions. The upper panel is for  $\alpha = 1$ , while the lower panel is for  $\alpha = 0.1$ .

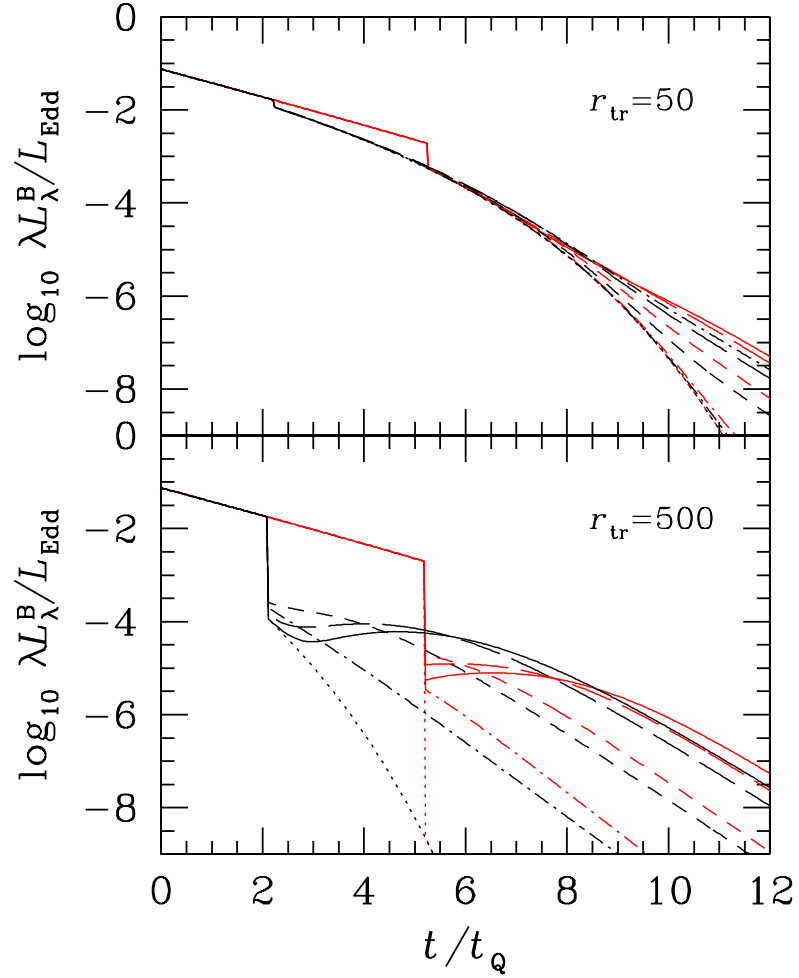


Fig. 3.— Spectral evolution of ADIOS+SD systems for  $\alpha = 1$  with different wind strengths ( $p_w = 0.1, 0.4$ , and  $0.9$ , respectively). The red lines correspond to the cases for  $\alpha = 0.1$ , while the black lines are for  $\alpha = 1$ . The solid lines represent the flows without winds ( $p_w = 0$ ). The long-dashed lines represent the weak wind cases ( $p_w = 0.1$ ). The short-dashed lines represent the medium wind cases ( $p_w = 0.4$ ). The dash-dotted lines represent the strong wind cases ( $p_w = 0.9$ ). The dotted lines represent the emission from the outer standard thin disk regions.

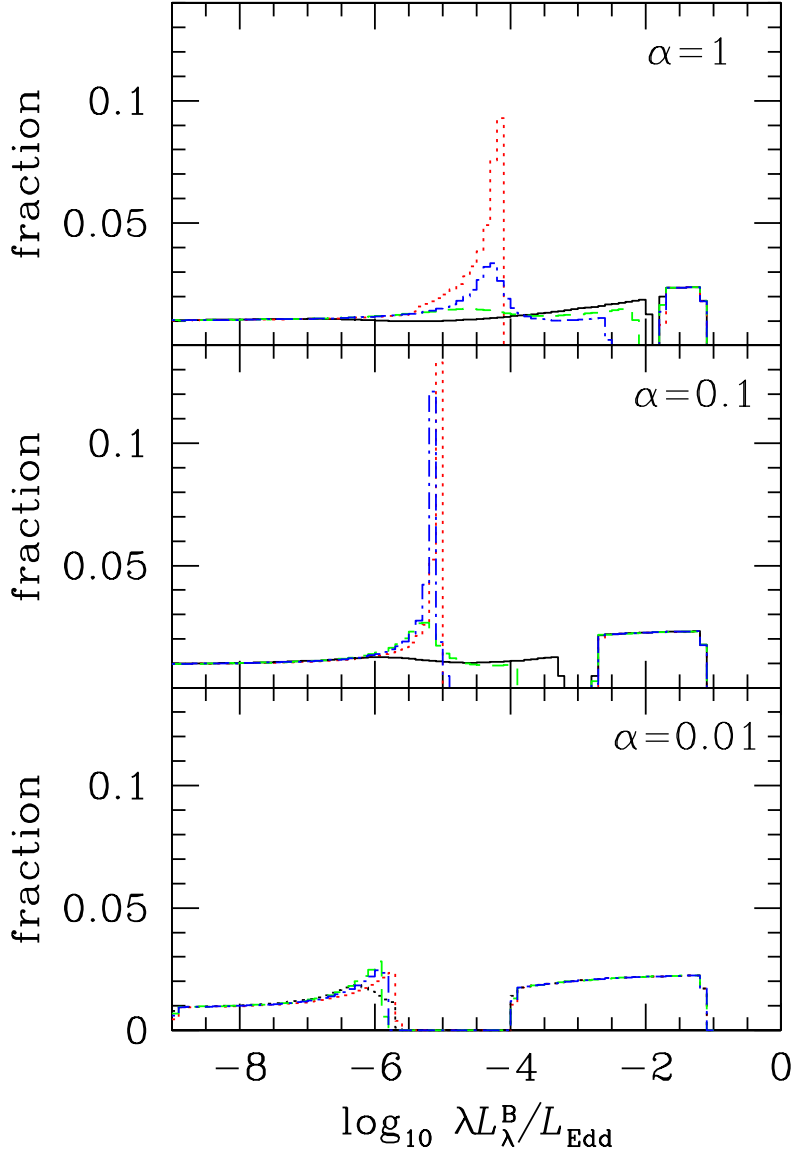


Fig. 4.— The distributions of Eddington ratio  $\lambda L_\lambda^B / L_{\text{Edd}}$  for different viscosity parameters:  $\alpha = 0.01, 0.1$ , and  $1$ , respectively. The dotted (red) lines are for the transitions of standard thin disks to pure-RIAFs. The solid lines represent the cases with  $r_{\text{tr}} = 50$ . The dashed (green) and dash-dotted (blue) lines represent  $r_{\text{tr}} = 100$  and  $200$ , respectively. The upper panel is for  $\alpha = 1$ , and the middle panel is for  $\alpha = 0.1$ , while the lower panel is for  $\alpha = 0.01$ .

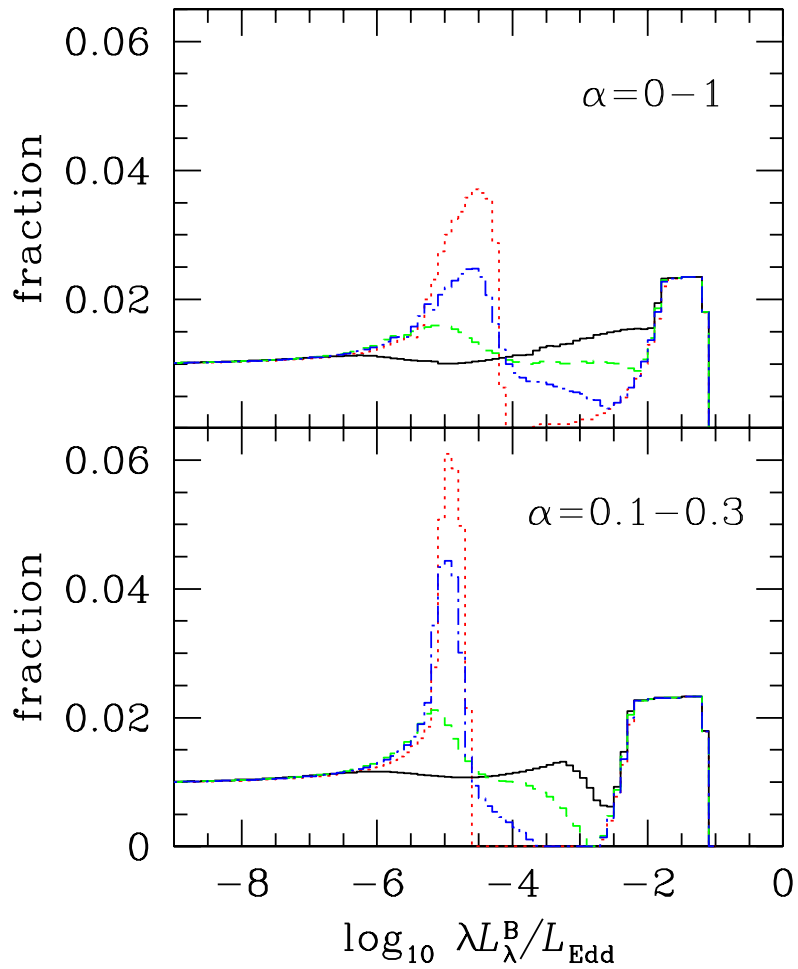


Fig. 5.— The distributions of Eddington ratio  $\lambda L_\lambda^B / L_{\text{Edd}}$  for the viscosity parameter  $\alpha$  randomly distributed in the range of  $0 - 1$  (upper panel), and  $0.1 - 0.3$  (lower panel), respectively. The dotted (red) lines are for the transitions of standard thin disks to pure-RIAFs. The solid lines represent the cases with  $r_{\text{tr}} = 50$ . The dashed (green) and dash-dotted (blue) lines represent  $r_{\text{tr}} = 100$  and  $200$ , respectively.

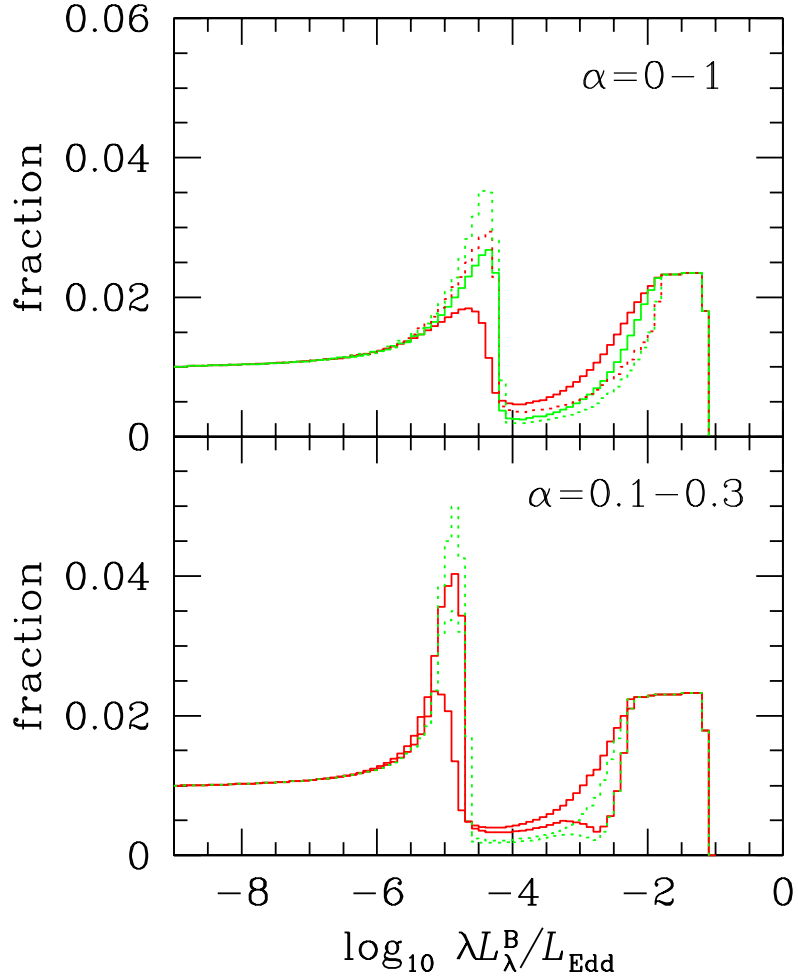


Fig. 6.— The distributions of Eddington ratio  $\lambda L_\lambda^B / L_{\text{Edd}}$  for the viscosity parameter  $\alpha$  randomly distributed in the range of 0 – 1 (upper panel), and 0.1 – 0.3 (lower panel), respectively. The simulations are carried out for different initial transition radii  $r_{\text{tr},0} = 10$  (solid lines) and 50 (dotted lines). The red and green lines represent  $p = 1$  and  $p = 2$ , respectively.

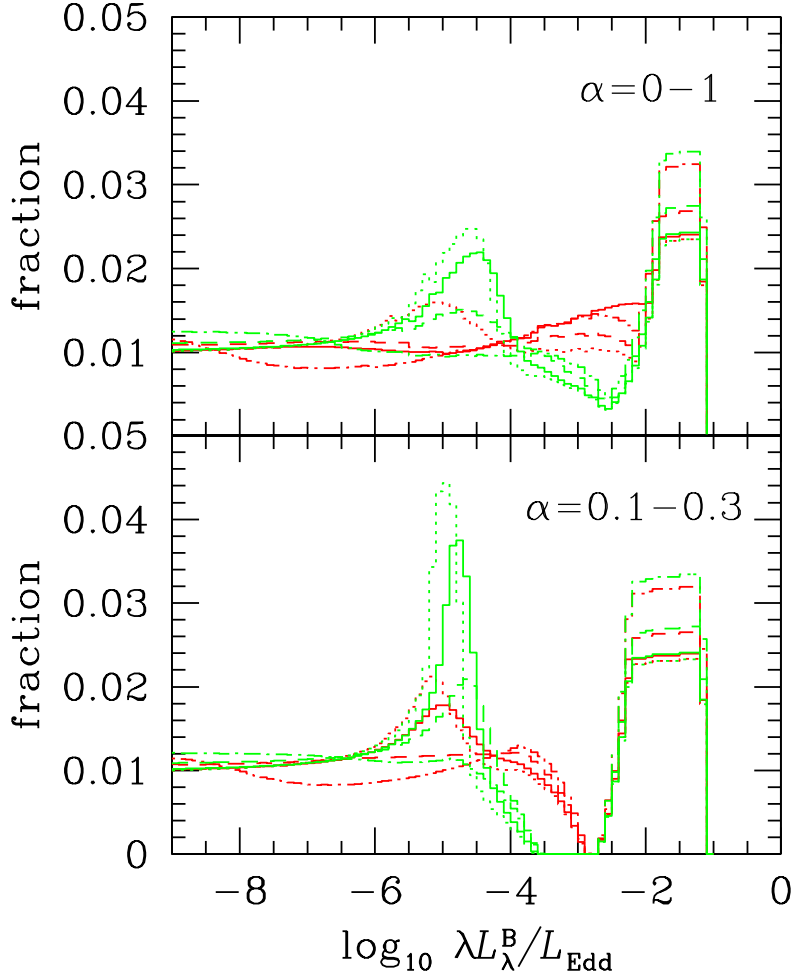


Fig. 7.— The distributions of Eddington ratio  $\lambda L_\lambda^B / L_{\text{Edd}}$  for the viscosity parameter  $\alpha$  randomly distributed in the range of  $0 - 1$  (upper panel), and  $0.1 - 0.3$  (lower panel), respectively. The simulations are carried out for ADIOS cases with fixed transition radii  $r_{\text{tr}} = 100$  (red lines) and  $200$  (green lines), respectively. The solid lines represent the weak wind cases ( $p_w = 0.1$ ), and the dashed lines represent the moderate wind cases ( $p_w = 0.4$ ), while the dash-dotted lines represent the strong wind cases ( $p_w = 0.9$ ). The dotted lines represent the the cases for  $p_w = 0$ .

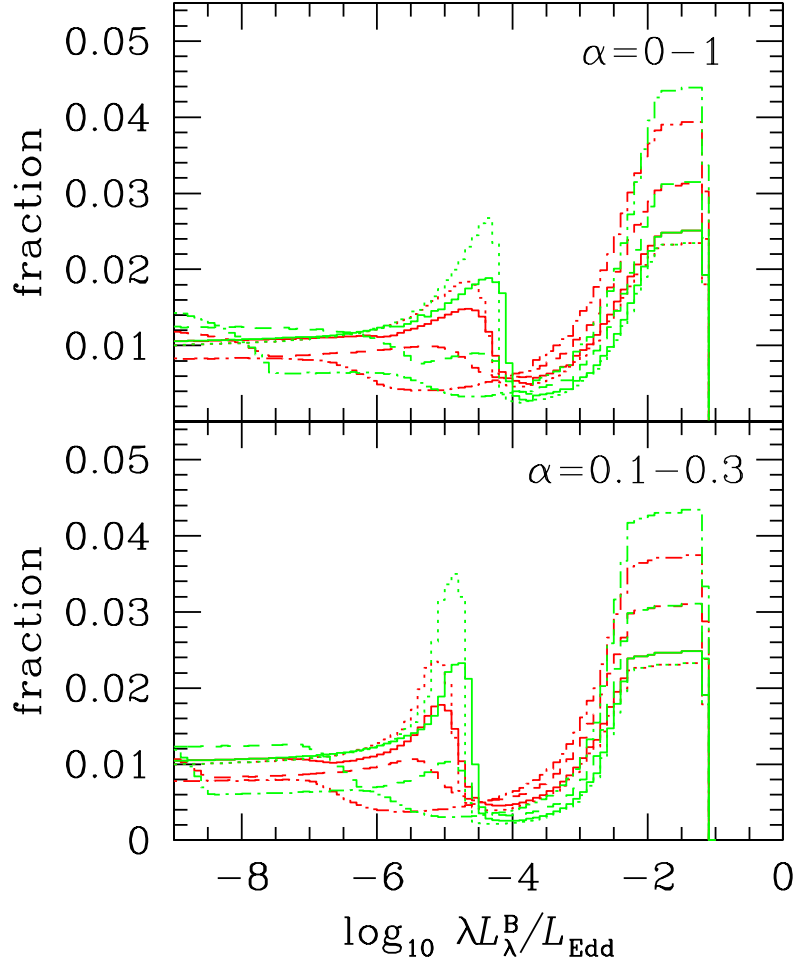


Fig. 8.— The distributions of Eddington ratio  $\lambda L_\lambda^B / L_{\text{Edd}}$  for the viscosity parameter  $\alpha$  randomly distributed in the range of  $0 - 1$  (upper panel), and  $0.1 - 0.3$  (lower panel), respectively. The simulations are carried out for the cases with  $p = 1$  (red lines) and  $p = 2$  (green lines), respectively. The initial transition radius  $r_{\text{tr},0} = 10$  is adopted in all simulations. The dotted lines represent for the cases of  $p_w = 0$ . The solid lines represent the weak wind cases ( $p_w = 0.1$ ) and the dashed lines represent the moderate wind cases ( $p_w = 0.4$ ), while the dash-dotted lines represent the strong wind cases ( $p_w = 0.9$ ).

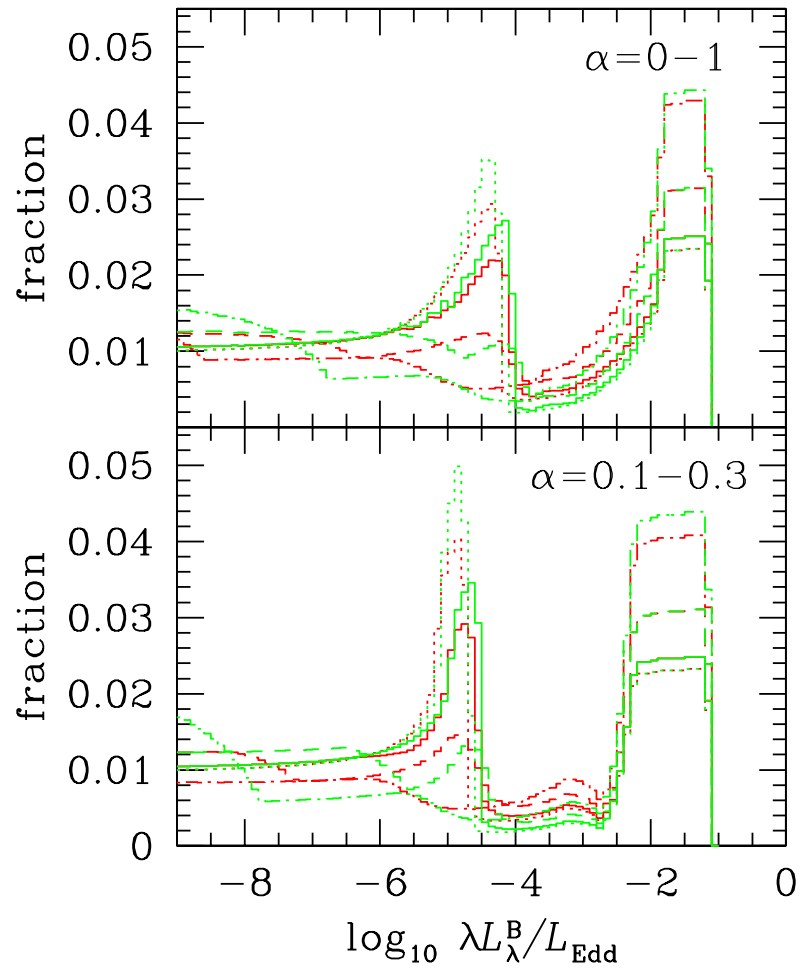


Fig. 9.— The same as Fig. 8, but for  $r_{\text{tr},0} = 50$ .

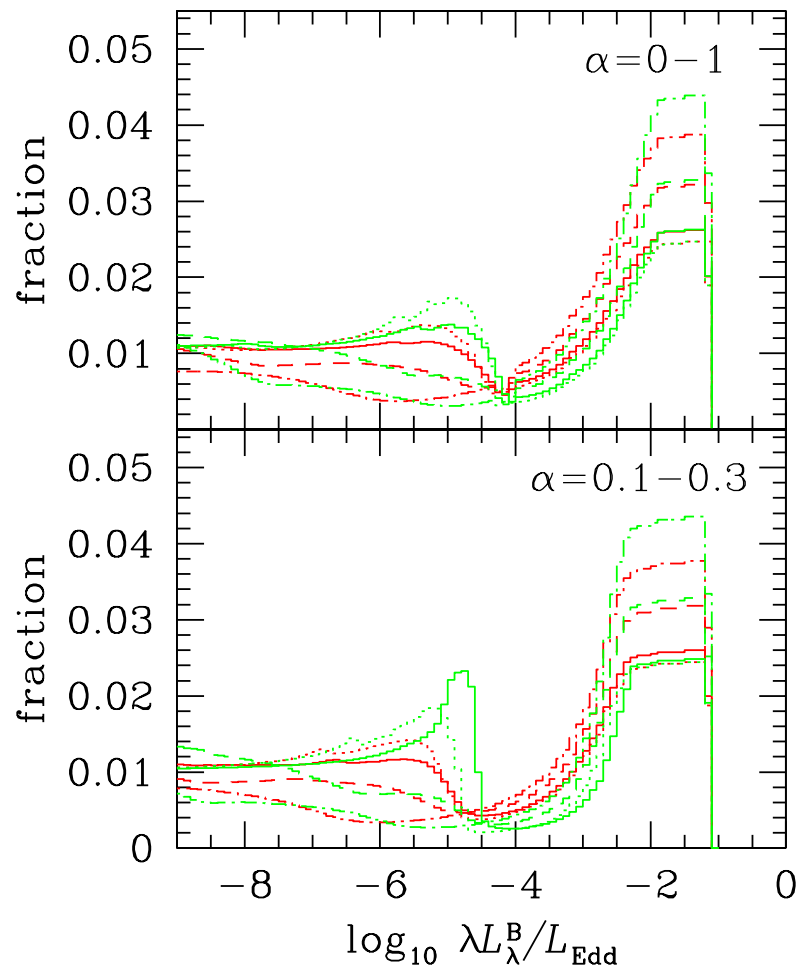


Fig. 10.— The same as Fig. 8, but the ratio of magnetic field pressure  $\beta$  is randomly distributed in the range of 0.5 – 1.

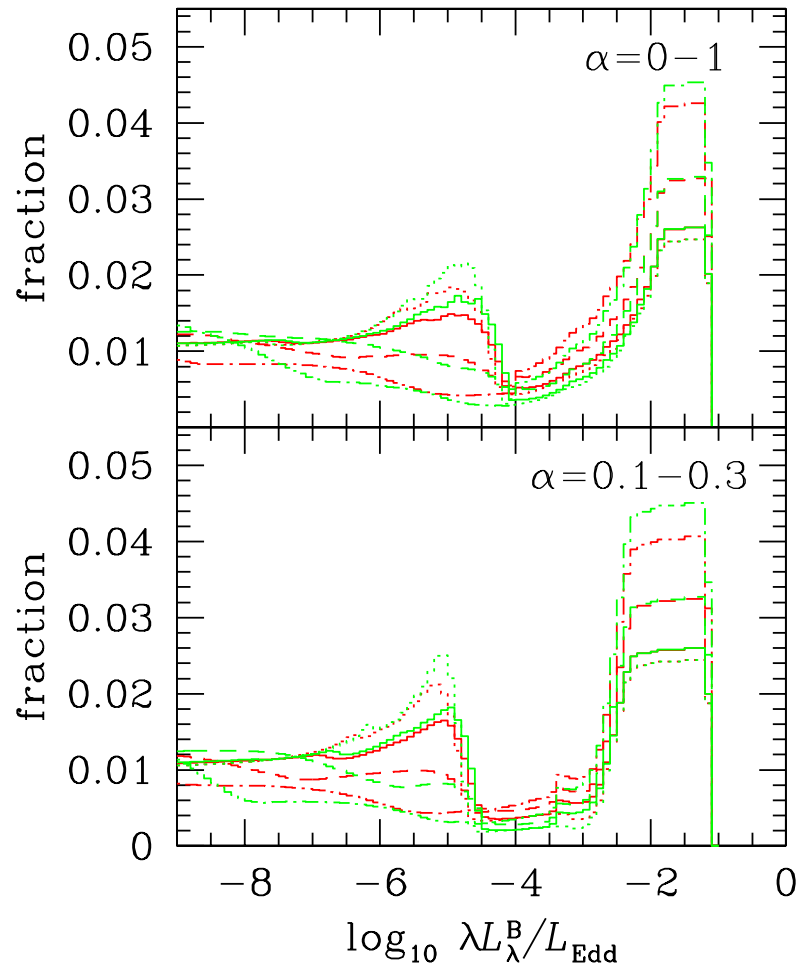


Fig. 11.— The same as Fig. 10, but for  $r_{\text{tr},0} = 50$ .

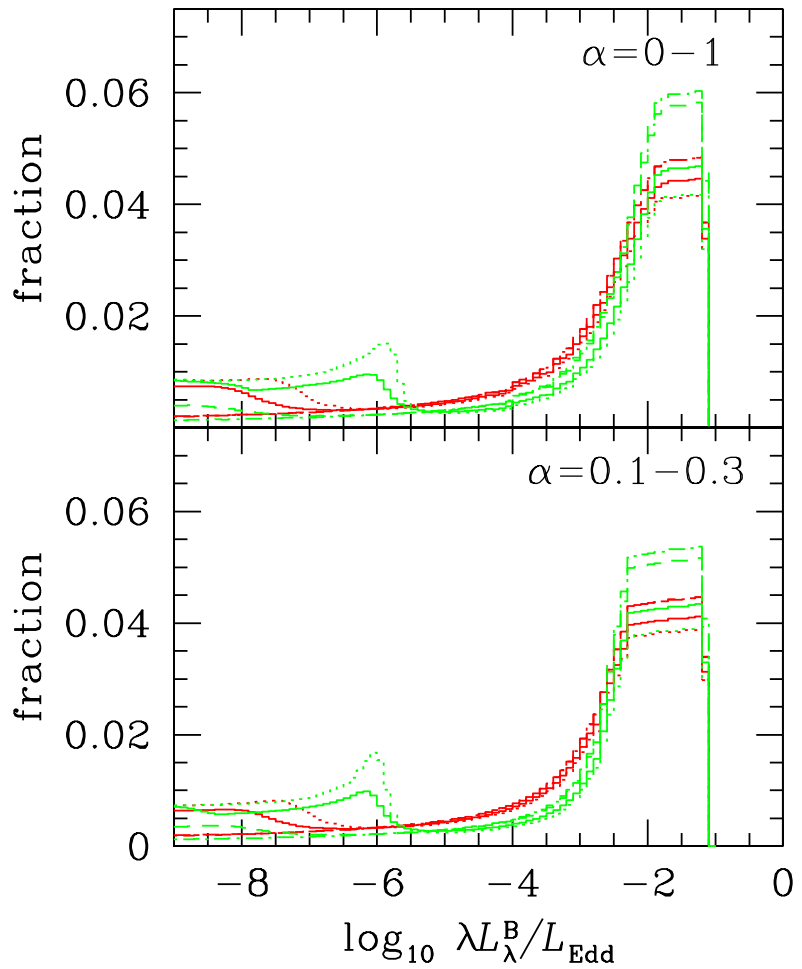


Fig. 12.— The same as Fig. 8, but for  $\delta = 1/2000$ .

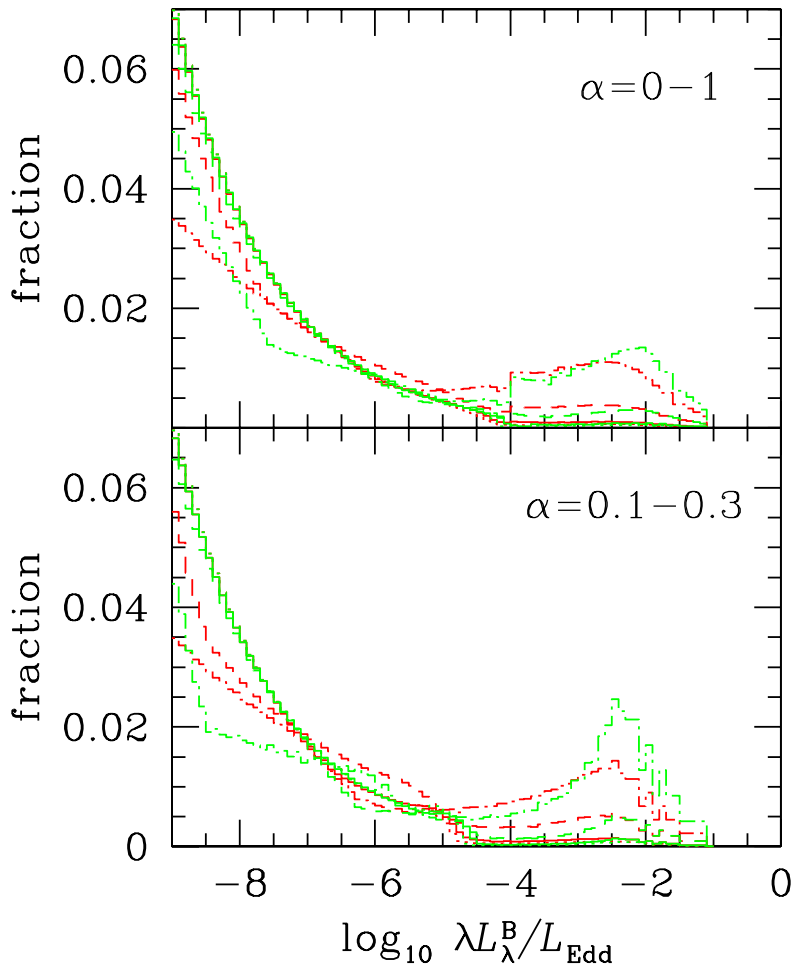


Fig. 13.— The same as Fig. 8, but for different time dependent accretion rate  $\dot{m}(t) = \dot{m}_{\text{crit}}(t=0)(1+t/t_Q)^{-\xi}$ , where  $\xi = 2$  is adopted.